# Augmenter of Liver Regeneration: A Flavin-Dependent Sulfhydryl Oxidase with Cytochrome *c* Reductase Activity†

Scott R. Farrell and Colin Thorpe*

*Department of Chemistry and Biochemistry, University of Delaware, Newark, Delaware 19716*

*Received September 22, 2004; Revised Manuscript Received November 15, 2004*

ABSTRACT: Augmenter of liver regeneration (ALR; hepatopoietin) is a recently discovered enigmatic flavin-linked sulfhydryl oxidase. An N-terminal His-tagged construct of the short form of the human protein has been overexpressed in *Escherichia coli*. Several lines of evidence suggest that, contrary to a recent report, human ALR is a disulfide-bridged dimer (linked via C15−C124) with two free cysteine residues (C74 and 85) per monomer. The C15−124 disulfides are not critical for dimer formation and have insignificant impact on the dithiothreitol (DTT) oxidase activity of ALR. Although the crystal structure of rat ALR shows a proximal disulfide (C62−C65) poised to interact with the FAD prosthetic group [Wu, C. K., Dailey, T. A., Dailey, H. A., Wang, B. C., and Rose, J. P. (2003) *Protein Sci. 12*, 1109−1118], only flavin reduction is evident during redox titrations of the enzyme. ALR forms large amounts of neutral semiquinone during aerobic turnover with DTT. This semiquinone arises, in part, by comproportionation between flavin centers within the dimer. Surprisingly, cytochrome *c* is about a 100-fold better electron acceptor for ALR than oxygen when DTT is the reducing substrate. These data suggest that this poorly understood flavoenzyme may not function as a sulfhydryl oxidase within the mitochondrial intermembrane space but may communicate with the respiratory chain via the mediation of cytochrome *c*.

Sulfhydryl oxidases catalyze the formation of disulfide bonds at the expense of molecular oxygen (*1*−*6*):

$$2R{-}SH + O_2 \rightarrow R{-}S{-}S{-}R + H_2O_2$$

Quiescin-like flavin-dependent sulfhydryl oxidase (QSOX)[1] enzymes are found in all multicellular organisms investigated to date (*6*−*10*). These proteins represent an ancient fusion (*9*) of thioredoxin modules with a domain termed ERV [essential for respiration and vegetative growth in yeast (*11*)] or ALR [augmenter of liver regeneration (*12*, *13*)]. A comparison of several sequences of this domain is presented in Figure 1.

Following the recognition that Quiescin Q6 was a flavin-dependent sulfhydryl oxidase (*10*), yeast ERV1p and ERV2p (*14*−*18*) and mammalian ALR (*19*) were found to be diminutive FAD-linked sulfhydryl oxidases. Crystal structures of ERV2p (*20*) and ALR (*21*) revealed a new helix-rich fold that houses the core sulfhydryl oxidase activity with a FAD binding site and a conserved proximal CxxC motif adjacent to the isoalloxazine ring. While ERV1p, ERV2p, and ALR appear to be relatively weak stand-alone sulfhydryl oxidases (*14*, *16*, *18*−*20*), the fusion with two thioredoxin domains in QSOX generates a facile, direct, catalyst for oxidation of a seemingly unlimited array of reduced proteins and peptides (*6*, *22*−*24*).

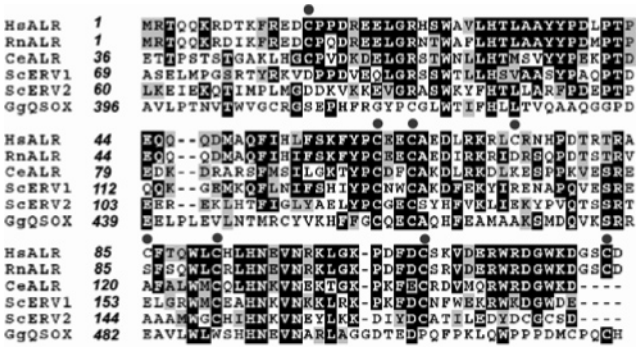


FIGURE 1: Sequence alignment of selected ALR, ERV, and QSOX proteins. Representative sequences of proteins homologous to ERV/ALR domains were chosen: human (Hs), rat (Rn), and *Caenorhabditis elegans* (Ce) ALR, *Saccharomyces cerevisae* (Sc) ERV1p and ERV2p, and *Gallus gallus* (Gg) QSOX. Boxshade was used for alignment. Cysteine residues in hsALR are highlighted with solid circles. The structural disulfide C91−108 in hsALR is conserved in ScERV1 and ScERV2 but not in QSOX (see later).

These sulfhydryl oxidases have a range of cellular locations. QSOX enzymes have been reported in the ER of multicellular organisms (*6*, *7*), within the Golgi (*25*), at the plasma and nuclear membranes (*7*), and secreted from the cell (*6*, *8*, *26*, *27*). ERV2p is found largely in the ER of yeast (*15*, *18*, *28*) where it participates in oxidative protein folding. In contrast, ALR is located primarily in the mitochondrial intermembrane space, as is its direct counterpart in yeast (the essential protein ERV1p) (*17*, *29*, *30*). At this location, ERV1p is involved in some aspect of the assembly or

† This work was supported in part by NIH Grant GM26643.

* Author to whom correspondence should be addressed. Phone: (302) 831-2689. Fax: (302) 831-6335. E-mail: cthorpe@udel.edu.

[1] Abbreviations: ALR, augmenter of liver regeneration; CTAB, cetyltrimethylammonium bromide; DTT, dithiothreitol; ER, endoplasmic reticulum; ERV, protein essential for respiration and viability in yeast; GSH, reduced glutathione; QSOX, flavin-dependent sulfhydryl oxidases homologous to Quiescin Q6; SOD, superoxide dismutase; Trx, thioredoxin; TrxR, thioredoxin reductase; NADPH, reduced nicotinamide adenine dinucleotide phosphate.

10.1021/bi0479555 CCC: $30.25 © 2005 American Chemical Society
Published on Web 01/14/2005

trafficking in Fe/S centers destined for cytosolic Fe/S proteins (*17*). Mammalian ALR has also been found in the cytosol (*31*), in the nucleus (*31*, *32*), and as a secreted growth factor (*33*−*36*). ALR appears to have multiple roles in the regulation of cell growth and differentiation (*17*, *19*, *30*, *33*−*35*, *37*, *38*).

This unusual diversity of proposed functions for ALR makes it the most enigmatic of those sulfhydryl oxidases, which show homology with QSOX. Here, we build upon the pioneering work of Lisowsky and colleagues on the ALR/ERV1p family with a further characterization of human ALR. Our work on the fundamental redox behavior of ALR has also uncovered an intriguing new activity of ALR of possible relevance to some of its physiological functions.

## MATERIALS AND METHODS

*Materials*. A pT7T3D plasmid containing the short-form ALR sequence was obtained through the IMAGE Consortium. The plasmid was amplified in Top10 *Escherichia coli* cells and harvested using a Qiaprep Spin miniprep kit. For cloning the long His-tagged linker, the sense primer 5′-CTGGAATTCATGCGGACGCA-3′, was used to incorporate an *Eco*RI restriction site at the 5′ end of the ALR sequence. For the short-linker His-tagged enzyme, the sense primer 5′-CTGGCTAGCATGCGGACGCA-3′ introduced an *Nhe*I restriction site. In both cases, the antisense primer 5′-CTGAAGCTTCTAGTCACAGG-3′ encoded a *Hin*dIII restriction site at the 3′ end of the ALR sequence. PCR products were purified using a Qiagen PCR purification kit and digested with appropriate restriction enzymes at 37 °C. PTrcHis (Invitrogen) was digested with the same restriction enzymes. The DNA was ethanol precipitated, redissolved in buffer, and ligated overnight with T4 Ligase at 4 °C. The plasmid was ethanol precipitated, suspended in water, and used to transform BL21(DE3) chemically competent cells (Invitrogen). Several colonies were picked for sequencing. Glycerol stocks were made and stored at −80 °C.

*General Methods*. Unless otherwise stated, all buffers were 50 mM potassium phosphate, pH 7.5, containing 0.3 mM EDTA. Visible and ultraviolet spectra were recorded on Hewlett-Packard 8452A or 8453 diode array spectrophotometers. Concentrations of ALR were expressed using a molar extinction coefficient of 11.6 $mM^{-1}$ $cm^{-1}$ at 456 nm for the enzyme-bound flavin determined upon release of free FAD with 0.5 mM cetyltrimethylammonium bromide (CTAB). Anaerobic methods were as described previously (*5*). ALR was photoreduced anaerobically 4 cm from a 150 W flood lamp using 1.0 $\mu$M 5-deazaflavin and 1 mM EDTA in phosphate buffer. All stoichiometries reported are on a per flavin (per subunit) basis. Gel filtration was performed at a flow rate of 1.0 mL/min on a Superdex 200 HR 10/30 column from Pharmacia using an Äkta FPLC. A homology model of human ALR was constructed using Swiss PDB viewer with the rat ALR coordinates (1OQC). Structures were visualized with DS ViewerPro (Accelerys).

*Determination of Midpoint Potentials for ALR.* Solutions of 15 $\mu$M of the C74−85 double mutant short-form ALR in 0.8 mL of phosphate buffer containing 2 $\mu$M methyl viologen were deoxygenated in dim light in the presence of 15 $\mu$M of one of the following redox dyes: indigo disulfonate (−121 mV), anthraquinone-2,6-disulfonate (−184 mV), anthraquinone-2-sulfonate (−226 mV), or phenosafranine (−252 mV). After an initial spectrum was recorded, the mixture was progressively reduced by the addition of aliquots of dithionite. Subsequent spectra were recorded after redox equilibration (typically <6 min) and stored for analysis. Anthraquinone-2,6-disulfonate had a redox potential which closely matched the short-form ALR. Here, the 2-electron reduction of ALR was followed at 456 nm and the dye at 341 nm. The resulting linear plots of log [oxidized]/[reduced] enzyme versus log [oxidized]/[reduced] dye yielded a midpoint potential for ALR of −178 ± 2 mV (four determinations).

*Assays.* ALR was assayed in a Clarke-type oxygen electrode (YSI 5331) and oxygen monitor (YSI 5300) in 2 mL of air-saturated 50 mM potassium phosphate (pH 7.5, 0.3 mM EDTA, 25 °C). A background trace followed the nonenzymatic oxidation of thiol before the addition of enzyme. Thiol substrates were prepared freshly in distilled water and were standardized using DTNB.

*Protein Expression.* Starter cultures (5 mL in Luria−Bertani media containing 50 $\mu$g of ampicillin/mL) were grown overnight at 37 °C and used to inoculate each of four 2 L flasks containing 500 mL of the same media supplemented with 5 $\mu$M riboflavin. When the absorbance at 600 nm reached 0.6, the cells were induced with 1 mM IPTG and incubated for an additional 5.5 h at 37 °C. Cells were harvested at 4000*g* for 30 min at 4 °C.

*Preparation of Extract.* Cells (10 g) were resuspended in 25 mL of 50 mM potassium phosphate buffer, pH 7.5, containing 300 mM NaCl, 0.1 mg/mL lysozyme, and general-use protease inhibitor cocktail (Sigma). The cells were disrupted with two passes through a French press at 10000 psi. After brief sonication to shear DNA, the cell lysate was centrifuged at 6000*g* for 30 min.

*Refolding of Long Peptide Linker ALR.* ALR with the long peptide linker (see above) forms inclusion bodies. After centrifugation, the cell debris was resuspended in 25 mL of 50 mM phosphate buffer, pH 7.5, without EDTA but containing 8 M urea, 10 mM DTT, and 2 mM FAD. The resulting suspension was dialyzed for a total of 22 h against two changes of the same buffer without additions and then centrifuged at 6000*g*.

*Purification of ALR with Long and Short Peptide Linkers.* The crude cell extract, or the reconstituted inclusion body dialyzate, was made 10 mM in $\beta$-mercaptoethanol and mixed with Invitrogen probond resin (1 mL of resin for every 8 mL of solution). After mixing end over end for 1 h at 4 °C, the resin was loaded into a column and washed with 4 mL aliquots of the following solutions: three washes of 50 mM phosphate containing 300 mM NaCl, 10 mM $\beta$-mercaptoethanol, and 10 mM imidazole, pH 7.5; three washes of the same solution without NaCl; and one wash omitting $\beta$-mercaptoethanol. The column was then developed with single 5 mL aliquots of phosphate buffer without salt or $\beta$-mercaptoethanol containing 50, 200, and 500 mM imidazole. ALR elutes as a bright yellow band in 200 mM imidazole and was immediately desalted using PD-10 columns equilibrated with 50 mM phosphate buffer, pH 7.5, containing 0. 3 mM EDTA. ALR was stored routinely at 4 °C. To ensure maximal flavin loading, ALR was incubated before use at 4 °C in anaerobic buffer containing 5 mM DTT and an equimolar concentration of free FAD. After at least 1 h, excess unbound FAD was removed by gel filtration on a

PD10 column equilibrated with aerobic phosphate buffer. During gel filtration the blue semiquinone form of ALR rapidly reverts to the bright yellow color of the oxidized protein.

*Mutation Studies of ALR.* Cysteine to alanine mutations used Quickchange site-directed mutagenesis (Stratagene). The primers (Integrated DNA Technologies) were as follows: C15A, 5′-GTTTAGGGAGGACGCCCCGCCG-GATCGCG-3′ and 5′-CGCGATCCGGCGGGGCGTCCTC-CCTAAAC-3′; C124A, 5′-GGAAGGATGGCTCCGCT-GACTAGAAGCTTGGC-3′ and 5′-GCCAAGCTTCTAGT-CAGCGGAGCCATCCTTCC-3′; C74A, 5′-CCTAA-GAAAAAGGCTGGCCAGGAACCACCCAGAC-3′ and 5′-GTCTGGGTGGTTCCTGGCCAGCCTTTTTCTTAGG-3′;C85A,5′-CCCGCACCCGGGCAGCCTTCACACAGTGGC-3′ and 5′-GCCACTGTGTGAAGGCTGCCCGGGTGCGGG-3′.

*Isolation of ALR Peptides.* ALR was alkylated at 25 °C in phosphate buffer containing 3 mM iodoacetic acid following the thiol titer using DTNB. After 6 h, excess iodoacetate was removed by washing the fully alkylated protein with 20 mM ammonium bicarbonate in a Centricon 30 concentrator. The protein solution was made 0.1% in SDS, boiled for 5 min, and digested at 25 °C with 3% w/w trypsin. Peptides were separated using a Hewlett-Packard series 1100 HPLC with a Phenomenex Jupiter C18 300A 250 × 4.60 mm, 5 $\mu$m column. Molecular weights were determined using a Maldi Omniflex NT and TOF MS ESI.

*Stopped-Flow Spectrophotometry.* Reactions were followed at 25 °C in a Hi-Tech Scientific SF-61 SX2 double-mixing stopped-flow system using software from Hi-Tech. Prior to anaerobic experiments, the driving syringes and flow cell were soaked for several hours with 10 mM dithionite solution. Solutions of DTT were prepared in phosphate buffer and standardized with DTNB. Two-electron reduced ALR was prepared in a tonometer and mixed with aerobic solutions made by mixing appropriate volumes of anaerobic and oxygen-saturated buffer (*39*). Cytochrome *c* turnover experiments were performed in double-mixing mode in aerobic solutions. ALR (syringe A) was first mixed with DTT (syringe B) and after 50 ms mixed with cytochrome *c* (syringe C) and buffer or superoxide dismutase (syringe D) to give final concentrations of 2.5 $\mu$M ALR, 2 mM DTT, 0−50 $\mu$M cytochrome, and 0 or 10 units/mL superoxide dismutase in phosphate buffer, 25 °C. Initial rates were determined and $k_{cat}$ and $K_m$ values estimated by nonlinear regression.

## RESULTS AND DISCUSSION

*Construction, Expression, and Purification of Human ALR.* The majority of the published work on ALR, including the recent crystal structure (*21*), has been performed with the short form of the protein which lacks an 80-residue extension at its N-terminus. For our initial characterization of the redox behavior of ALR, we have chosen this form because it can be readily expressed heterologously in *E. coli* (*19*) and it allows a ready comparison with earlier work. In these prior studies, His tags have been appended to either the N- or C-termini of mammalian ALR (*19*). We have largely used an N-terminal tag, MGGSHHHHHHGMAS, identical to that chosen for crystallization trials of the rat ALR protein (*40*).

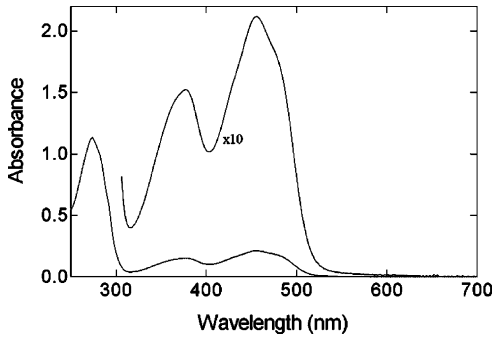


FIGURE 2: UV/vis spectrum of recombinant human ALR. To maximize flavin content and minimize turbidity, ALR was incubated anaerobically for 1 h at 4 °C in 50 mM phosphate buffer, pH 7.5, 25 °C, containing 0.3 mM EDTA, 5 mM DTT, and 100 $\mu$M FAD. The mixture was then gel-filtered and the spectrum of 18.3 $\mu$M ALR measured immediately at 25 °C. The upper curve is amplified 10-fold to show details of the flavin spectrum.

However, some preliminary experiments were conducted with a longer N-terminal linker (see Materials and Methods). To date, we have observed no significant differences in catalytic or redox behavior between the two tagged forms. The shorter construct typically gave 25−30 mg of >95% purified protein/L of medium. Approximately 85% of the protein induced by IPTG was found to be soluble under the growth conditions used (see Materials and Methods). In contrast, the longer linker ALR construct formed inclusion bodies in *E. coli* and was refolded and reconstituted with flavin before purification as described in Materials and Methods. It proved very prone to reaggregation and was only used in initial experiments.

*Preliminary Characterization of Human ALR.* Figure 2 shows a UV/vis spectrum of the short-linker recombinant enzyme. The spectrum is weakly resolved in the flavin region with peaks at 456 and 376 nm, somewhat different from the 450 and 360 nm reported earlier for the rat short-form ALR (*19*). The molar extinction coefficient for the bound FAD moiety in human ALR was experimentally determined to be 11600 ± 100 $M^{-1}$ $cm^{-1}$ at 456 nm after the addition of 0.5 mM CTAB (see Materials and Methods). This value is significantly larger than a previously assumed value of 10000 $M^{-1}$ $cm^{-1}$ (*21*). Release of flavin, judged by the reversion to a spectrum of free FAD, was complete in less than 20 s (not shown). The 280/450 nm absorbance ratio of freshly prepared ALR was 4.8 (Figure 2). Human ALR shows negligible flavin fluorescence, amounting to less than 0.5% of an equivalent concentration of free FAD excited at 450 nm and emitting at 530 nm (not shown; see Materials and Methods). As expected, ALR shows a typical protein fluorescence exciting at 280 nm and emitting at 340 nm (not shown).

Our short-linker human protein is prone to slowly increasing turbidity upon storage under aerobic conditions. This does not reflect global denaturation, because the precipitate is bright yellow and none of the noncovalently bound flavin is released into solution (see later). Precipitation can be largely avoided by storing the protein under nitrogen, and it can be reversed after incubation with excess DTT. Figure 2 was recorded immediately after DTT pretreatment and gel filtration (see Materials and Methods). An alternate strategy to avoid aggregation is described later.

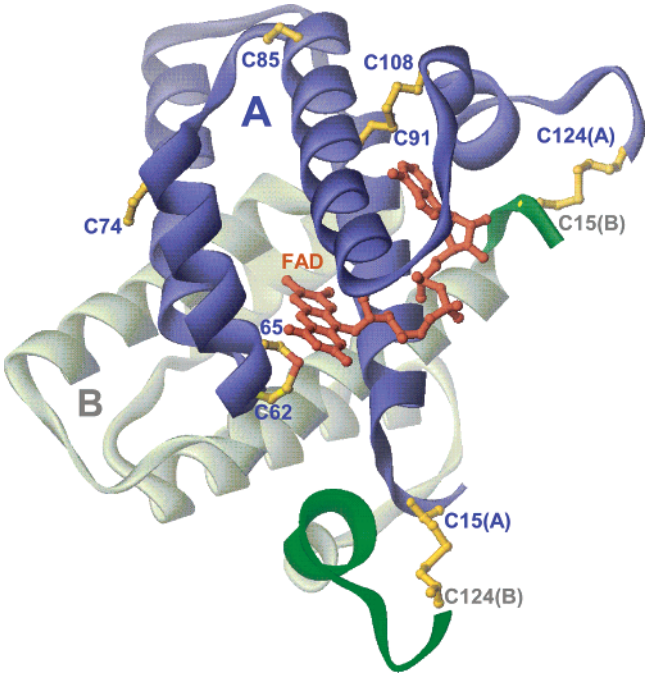


FIGURE 3: Homology model of human short-form ALR based on the crystal structure of rat ALR. The model was constructed using Swiss PDB viewer, and the coordinates were viewed by DS ViewerPro. Subunit A is shown in blue and subunit B in gray (with N- and C-termini highlighted in green). Cysteine and half-cysteine residues are numbered and shown in yellow. The FAD is in orange, as is the sulfur atom of C65 which likely participates in C4a adduct formation with the flavin. In subunit B the FAD is omitted, and only C15(B) and C124(B) are depicted.

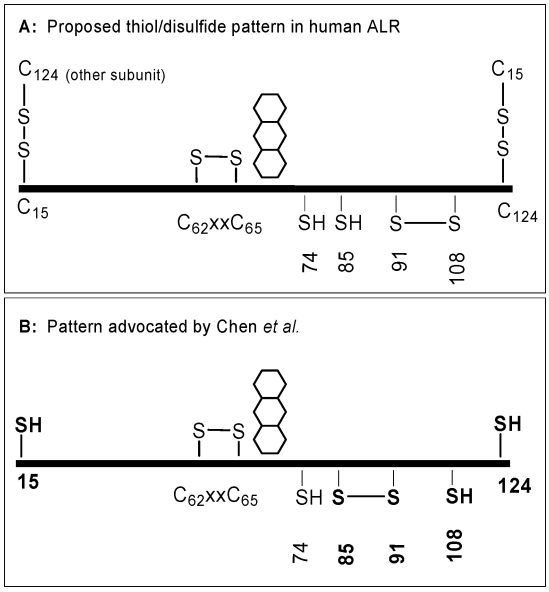


FIGURE 4: Cysteine residues and disulfide connectivity of human ALR. Panel A represents the pattern inferred from the crystal structure of rat ALR (see the text). Panel B is that proposed by Chen et al. (*38*). The flavin ring is shown schematically next to the proximal disulfide C62−65.

*Homology Model and Disulfide Connectivity in Human ALR.* Since human and rat ALR show about 86% sequence identity, a threaded minimized estimate of the structure of the dimeric human protein based on the rat structure (*21*) can be obtained with considerable confidence. This model (focusing on the blue subunit in Figure 3) shows that the conserved redox-active disulfide C62−65 is primed for communication with the flavin ring with the sulfur of C65 (orange) at a distance of 3.2 Å from the C-4a position of the isoalloxazine ring. A second disulfide (C91−108) is conserved in ERV1p, ERV2p, and mammalian ALR (Figure 1) and forms an apparent structural disulfide bond between a helix and a strand in the crystal structure of ERV2p (*20*) and ALR (*21*) (Figure 3). The third disulfide bond forms intersubunit links [C15−124 (*21*)] between the flexible N- and C-termini of the ALR structure (Figure 3). These two intersubunit disulfides (out of a total of six disulfide bridges in the dimer) are unique to ALR: they are not found in either its yeast homologue, ERV1p, or the ER-resident yeast protein, ERV2p. Unlike the rat and mouse enzymes, each subunit of human ALR contains two additional nonconserved free cysteine residues (C74 and C85) depicted at the top left of Figure 3 and, schematically, in Figure 4A.

A recent paper (*38*) proposed a pattern of disulfide bond connectivity in human short-form ALR that conflicts with that reported in the crystal structure of its rat counterpart (*21*). This alternative connectivity (Figure 4, panel B) was deduced from the mass of proteolytic peptides derived from ALR that was not alkylated prior to digestion. Unfortunately, confounding disulfide exchange reactions can readily occur in the presence of free thiols during denaturation and prolonged digestion. Notwithstanding this technical issue, the new proposed disulfide pattern seems highly unlikely a priori. First, a C85−91 disulfide bond could only apply to human ALR because the counterpart of C85 is not found in any other ALR sequenced to date. (For example, Figure 1 shows that this cysteine is replaced by a serine in rat ALR.) Second, the rearranged pattern would remove the conserved structural disulfide C91−108 in ERV/ALR family members (Figure 1) and replace it with C85−91. Third, the homology model in Figure 3 shows that the proposed C85−91 disulfide could not be accommodated within the α-helix that runs from residues 82−101 in ALR.

Experimental evidence is also inconsistent with the model in Figure 4B. Figure 4A predicts a free thiol titer of 2 per subunit (C74, C85), whereas panel B implies a total of four reduced cysteine residues (C15, C74, C108, C124). The reaction between 0.5 mM DTNB and short-linker human ALR is complete in less than 15 s at pH 7.5 and yields a stoichiometry of 2.0 free cysteines per monomer (see Materials and Methods). This rapidity suggests that both thiols are exposed to solvent; no further reaction occurs upon denaturation of ALR with either 0.5 or 5 mM CTAB (not shown). The facile reaction of two thiols is consistent with the evident solvent accessibility of both C74 and C85 in Figure 3 (solvent-accessible surface not shown). In accord with their nonconservation in ALR sequences (see earlier) the double mutant C74A/C85A gave fully active stable protein (see later). In addition, the double mutant showed essentially no reaction with DTNB (<0.2 reactive thiols per subunit; not shown) whereas the corresponding double mutant in Figure 4, panel B, would predict four free thiols per subunit.

Finally, Figure 4, panel B, omits the interchain disulfide bridges (C15−124) clearly evident in the crystal structure of rat ALR (*21*) and reproduced in the homology model of the human protein in Figure 3. Mutation of either C15 or C124 in human ALR to alanine results in a fully active

Table 1: DTT Oxidase Activity of Wild Type and Selected Cysteine Mutants of Human ALR

| ALR construct | linker | $k_{cat}$ ($min^{-1}$) | $K_m$ (mM) | $k_{cat}/K_m$ ($M^{-1}s^{-1}$) |
|---|---|---|---|---|
| wild type | short | 66 ± 6 | 2.1 ± 0.5 | 520 |
| C15A | short | 52 ± 2 | 1.3 ± 0.2 | 670 |
| C124A | short | 54 ± 2 | 1.8 ± 0.2 | 500 |
| C74A/C85A | short | 50 ± 3 | 2.0 ± 0.3 | 420 |
| C15A/C124A | long | 57 ± 3 | 2.0 ± 0.3 | 475 |
| C15A/C74A/C85A/C124A | long | 75 ± 3 | 1.7 ± 0.2 | 735 |

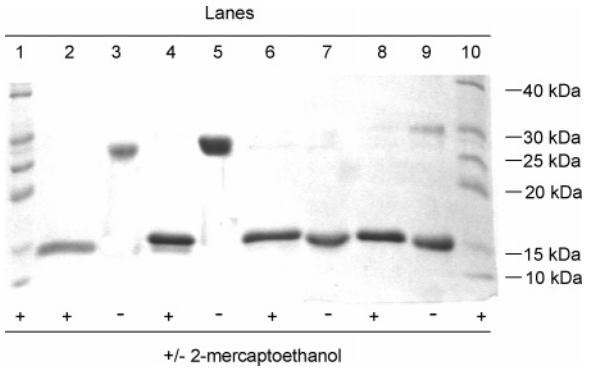


FIGURE 5: SDS−PAGE of recombinant wild-type ALR and selected cysteine to alanine mutants. Samples were run using an 18% cross-linked gel. All of the ALR samples ran in the 10−40 kDa region of the gel shown here. Lanes 1 and 10 were markers. ALR samples in even-numbered lanes from 2 to 9 were prereduced with 2-mercaptoethanol. Lanes: 2 and 3, wild-type ALR; 4 and 5, C74A/C85A double mutant; 6 and 7, C15A ALR; lanes 8 and 9, C124A ALR. The faint dimer formation in lane 9 may reflect a small amount of disulfide cross-linking after SDS denaturation in the absence of 2-mercaptoethanol.

enzyme (Table 1) that shows essentially the same visible spectrum as wild-type ALR (see later). Like the wild-type protein, both mutant proteins run on gel filtration under native conditions as dimers (not shown; see Materials and Methods). Both single mutant proteins show an approximate unit *increase* in thiol titer (from 2 of wild type to 3.0 and 3.1 per subunit for C15A and C124A, respectively; see Materials and Methods). These data can only be accommodated if both C15 and C124 participate in disulfide bonds.

Further, evidence supporting interchain bridges comes from SDS−PAGE of the protein constructs as described in Figure 5. Like a human ALR-GFP fusion reported by Lisowsky and colleagues (*19*), wild-type human ALR is a dimer in the absence of 2-mercaptoethanol but a monomer in its presence (lanes 3 and 2 of Figure 5, respectively). However, both C15A and C124A mutants run as monomers in the presence or absence of reductant (lanes 6−9 of Figure 5). In summary, the structural and biochemical evidence described above contradicts the model suggested by Chen et al. (*38*) and is completely consistent with the connectivity shown in panel A of Figure 4.

Finally, a general comment about the disulfide bonds in ALR is relevant here. It is unusual that an intracellular, but non-ER resident, eukaryotic protein contains structural disulfide bonds. The short form of ALR has apparently four per dimer. Surveys of disulfide bonds in proteins show that they are typically buried (>70% of them are solvent inaccessible) (*41*, *42*). However, a number of the disulfides of ALR appear solvent accessible (using a 1.4 Å probe radius; not shown), and it will be interesting to learn their redox state within the mitochondrial intermembrane space (see later).

*DTT Oxidase Activity of the Thiol Mutant of ALR.* Identification of the physiological substrate(s) for ALR represents an important unresolved issue (see later). In prior work, human ALR showed a turnover number of about four disulfides generated per minute using reduced lysozyme in 2 M urea (*43*). We have used DTT here because it gives turnover numbers in the 50−75/min range, is a convenient substrate, and provides a number of interesting insights into ALR catalysis. Table 1 shows that neither $k_{cat}$ nor $K_m$ for DTT oxidation shows large differences between wild-type and single, double, or quadruple cysteine mutant proteins. All of these constructs retain the active site CxxC motif. Lisowsky and colleagues (*19*), Chen et al. (*38*), and Wu et al. (*21*) have prepared both of these active site mutants and report that they show undetectable sulfhydryl oxidase activity. Accordingly, they have not been pursued here.

Two of the constructs in Table 1 have the longer N-terminal His tag (see above), but this makes little difference to DTT oxidase activity. Clearly, the free cysteines 74 and 85 are not essential for enzymatic activity toward DTT, consistent with their lack of conservation between rat and human sequences and their distance from the isoalloxazine ring (Figures 1 and 3). More significantly, the interchain disulfide Cys15−124 (Figure 3) is also not catalytically essential for the DTT oxidase activity measured here. Evidently this disulfide bond does not serve in a chain of disulfide bridges by relaying reducing equivalents to the proximal disulfide (C62−C65) in the way that the mobile CxC motif does in ERV2p (*20*).

*Rationale for Using the C74A/C85A Double Mutant of Human ALR.* As mentioned earlier, C74 and C85 in human ALR are not conserved in other ALRs and can both be mutated to alanine residues without significant impact on DTT oxidase activity. These two free surface-reactive cysteines cause slow aggregation of human short-form ALR under aerobic conditions. Thus the thiol titer drops from 2 per subunit to 1.1 over 1 day in aerobic buffer (pH 7.5, 0.3 mM EDTA, 4 °C), and progressive aggregation is evident from gel filtration, SDS−PAGE under nonreducing conditions, and light scattering experiments (not shown). While we can reverse this tendency of human ALR to self-oxidize using DTT or minimize the effect with storage under nitrogen, it proved more convenient to perform subsequent studies with the C74A/C85A double mutant (see Materials and Methods).

*Dithionite Titrations of ALR.* Figure 6 shows a dithionite titration of the human short-form double mutant ALR at pH 7.5 in the presence of methyl viologen to mediate transfer of reducing equivalents between reductant and the various redox forms of the protein. Complete reduction of the flavin requires about 2.3 electron equivalents of dithionite (see inset) with the clear intermediacy of significant levels of the blue neutral semiquinone. Assuming that the fully formed neutral semiquinone of ALR has an extinction coefficient of 4.4 $mM^{-1}$ $cm^{-1}$ at 570 nm (see later), about 25% of the flavin accumulates in the blue radical at the midpoint of flavin reduction. The behavior of ALR is unusual, since flavoprotein oxidases would be expected to form the red anionic flavin semiquinone (*44*, *45*). Comparable reductive titrations of ALR up to pH 9.0 provide no significant

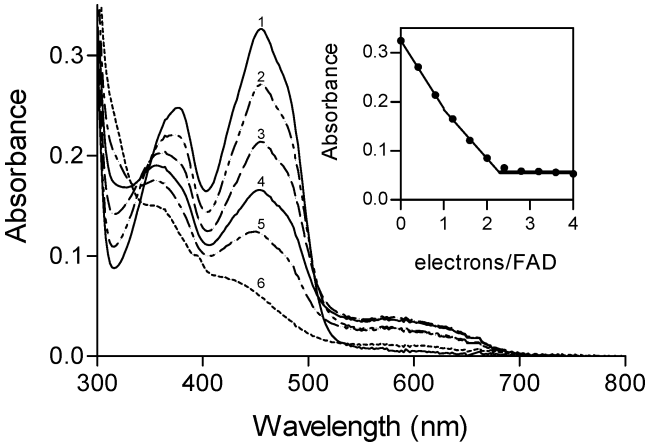


FIGURE 6: Dithionite titration of the C74A/C85A double mutant of human ALR. The double mutant (28 $\mu$M in 50 mM phosphate buffer, pH 7.5, containing 0.3 mM EDTA and 1 $\mu$M methyl viologen) was made anaerobic (curve 1; see Materials and Methods) and titrated with 0.4, 0.8, 1.2, 1.6, and 2.8 electron equivalents of dithionite per subunit (curves 2−6, respectively). Intermediate spectra are omitted for clarity. The inset plots absorbance at 456 nm as the titration proceeds.

evidence of red anionic semiquinone (not shown). After the addition of about 2.3 electrons, a stable methyl viologen radical appears, as judged by a significant shoulder at 390 nm and new absorbance at 580 nm (not shown). Clearly, only the flavin center of ALR and not, additionally, the proximal disulfide is reduced under these conditions.

The midpoint potential for human short-form double mutant ALR was established by repeating dithionite titrations in the presence of a range of redox dyes (see Materials and Methods). Four independent experiments with anthraquinone-2,6-disulfonate ($E_m = -184$ mV) gave a midpoint potential of $-178 \pm 2$ mV for the 2-electron reduction of this form of ALR. The redox-active disulfide (C62−65, Figure 3) must clearly have a considerably more negative potential, since we have been unable to reduce this center during the reductive titrations of this study.

*Photochemical Reduction.* A similar picture to the dithionite titration of Figure 6 emerges from catalytic photoreduction using deazaflavin (see Materials and Methods). First, the flavin of ALR was completely reduced (curve 1 of Figure 7); further anaerobic illumination had no apparent effect on the visible spectrum of the enzyme (or the subsequent stoichiometry of oxidative titrations; not shown). The solution was then titrated with standardized anaerobic potassium ferricyanide. Reoxidation was complete upon the removal of 2 electrons per flavin (Figure 7, curve 8 and inset). At intermediate stages of the titration very similar levels of blue flavin semiquinone are encountered to those seen in Figure 6.

As observed in Figure 6, the redox potentials of the flavin and of the proximal disulfide C62−65 appear widely separated, allowing essentially stoichiometric reduction of the flavin without significant accumulation of 4-electron reduced protein. The long wavelength absorbance seen in Figures 6 and 7 has the fine structure expected for a blue neutral semiquinone radical (see later); the feature is clearly not that of a charge-transfer interaction between oxidized flavin and a proximal thiolate as observed with QSOX (*5*, *21*, *23*) or members of the pyridine nucleotide dependent disulfide oxidoreductases (reviewed in ref *46*).

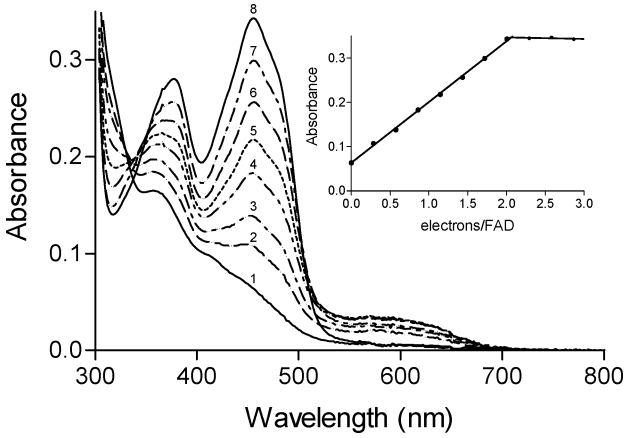


FIGURE 7: Reoxidation of photochemically reduced human ALR. Curve 1: an anaerobic solution of 30 $\mu$M ALR was photoreduced with 5-deazaflavin (for 25 min; see Materials and Methods) and titrated with 0.29, 0.57, 0.86, 1.15, 1.43, 1.72, and 2.00 electron equivalents of ferricyanide (curves 2−8). The inset plots the absorbance changes at 456 nm against titrant added.

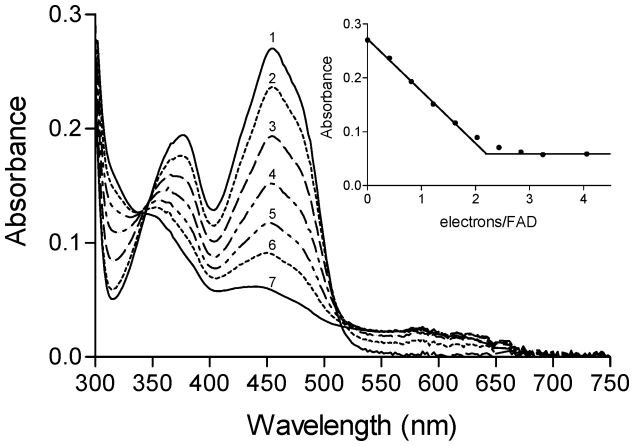


FIGURE 8: Anaerobic titration of ALR with DTT. Oxidized ALR (curve 1: 23 $\mu$M in 50 mM phosphate buffer, pH 7.5, containing 0.3 mM EDTA) was titrated anaerobically at 25 °C with 0.4, 0.8, 1.2, 1.6, 2.0, and 3.2 electron equivalents from DTT (curves 2−7, respectively). Intermediate spectra are omitted for clarity. The inset plots the absorbance change at 456 nm during the titration.

*DTT Reduction under Anaerobic and Aerobic Turnover Conditions.* Figure 8 shows that 1 equiv of DTT (2 electron equivalents per subunit; see inset) effects almost complete reduction of the flavin prosthetic group of human ALR. Unlike photochemical reduction (e.g., Figure 7, curve 1), significant levels of the blue radical persist even upon the addition of excess DTT (Figure 8, curve 7). However, much higher levels of the blue neutral semiquinone are observed during DTT turnover in aerobic buffer (Figure 9). Here, oxidized ALR was mixed with 10 mM DTT at pH 7.5, and the spectral changes were followed in the diode array spectrophotometer. The inset in Figure 9 shows that the blue semiquinone increases in a reaction that is half-complete about 19 s after the addition of DTT. At this pH, bleaching at 456 nm largely precedes the appearance of the blue semiquinone. A somewhat smaller level of neutral radical was observed at pH 7.0 by Wu et al. during their crystallographic investigations of the structure of recombinant rat ALR (*21*).

One explanation for the appearance of the radical upon the addition of a formal 2-electron reductant (DTT) is that

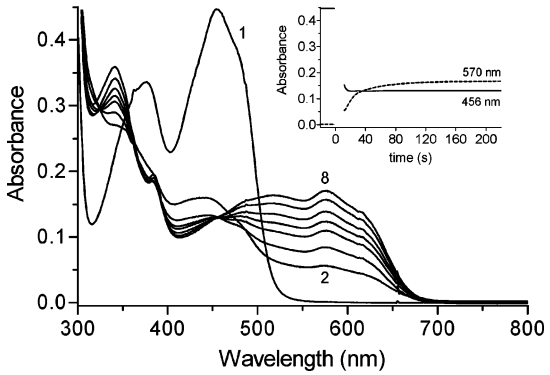


FIGURE 9: Enzyme-monitored turnover of DTT. ALR (38.5 $\mu$M in 0.8 mL of phosphate buffer, pH 7.5, 25 °C) was mixed at time zero with 10 mM DTT. Only selected spectra are shown for clarity. The inset plots absorbance changes at 456 and 580 nm.

it reflects a comproportionation reaction: either between two separate ALR dimers or via electron transfer across subunits within the same dimer (depicted as I or II):

$$\text{I: } ALR_{dimer}\cdot Fl_{2e} + ALR_{dimer}\cdot Fl_{ox} \leftrightarrow 2ALR_{dimer}\cdot Fl^{\bullet}$$

$$\text{II: } ALR_{subunit\ A}\cdot Fl_{2e}/ALR_{subunit\ B}\cdot Fl_{ox} \leftrightarrow ALR_{subunit\ A}\cdot Fl^{\bullet}/ALR_{subunit\ B}\cdot Fl^{\bullet}$$

To assess the rate of reaction I, we mixed 2-electron reduced ALR (generated photochemically; see Materials and Methods) anaerobically with an equimolar concentration of oxidized ALR. Comproportionation equilibration yields the level of semiquinone seen in Figures 6 and 7 with a half-time of 6.6 min at 25 °C (not shown). This rate is too slow to account for the comparatively rapid appearance of blue semiquinone observed in the inset to Figure 9.

Dutton and colleagues have argued that electron transfer rates between redox centers are comparatively little influenced by the medium which separates them but strongly influenced by driving force and edge to edge distance between reacting groups (*47*, *48*). In dimeric ALR the closest distance between isoalloxazine rings A and B is about 19 Å, and this would correspond to an isopotential electron transfer rate of about 10/s (*48*; this is roughly 10-fold faster than catalytic turnover; Table 1). Even if this theoretical rate were overestimated by 100-fold, it would still be fast enough to account for the appearance of blue semiquinone in Figure 9. Thus comproportionation in ALR is likely dominated by electron tunneling across the dimer interface because of the relative proximity of the two flavin rings.

*A New Enzymatic Activity for ALR.* We considered another possible explanation for the appearance of the flavin semiquinone in Figure 9: that it is the consequence of 1-electron reduction of dioxygen during turnover of DTT. The experiments described below show that this is not the case and have led to the discovery of a new enzymatic activity of ALR.

McCord and Fridovich and Massey et al. showed that a number of flavoproteins are weak de facto cytochrome *c* reductases because they nonphysiologically leak traces of superoxide during aerobic turnover (*49*−*51*). Two examples from this early work are particularly relevant because they are members of the pyridine nucleotide disulfide oxidoreductase family and contain flavin in close communication with

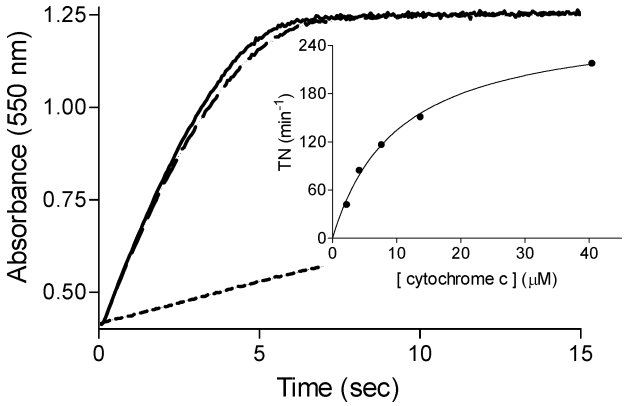


FIGURE 10: ALR-mediated reduction of cytochrome *c*. In a double-mixing experiment, cytochrome *c* was first mixed with DTT and subsequently with ALR and/or SOD. The main panel plots the absorbance at 550 nm using 40 $\mu$M cytochrome *c* with 2.5 $\mu$M ALR alone (solid line), with the additional presence of 10 units/mL SOD (long dashed line), or including SOD, but omitting ALR, to record the nonenzymatic reduction of cytochrome by DTT (short dashed line). Concentrations are those after double mixing (throughout 2 mM DTT in 50 mM phosphate buffer, pH 7.5, containing 0.3 mM EDTA at 25 °C). Initial rates, corrected for nonenzymatic reduction, are plotted as a function of cytochrome concentration in the inset. The line is a fit to a $k_{cat}$ of 270/min and a $K_m$ of 10 $\mu$M.

a redox-active disulfide (*46*). The NADH-dependent cytochrome *c* reductase activity of lipoamide dehydrogenase (2.7 mol of cytochrome *c* reduced/min) was inhibited by 90% on the addition of superoxide dismutase (SOD). Similarly, glutathione reductase catalyzes the NADPH-dependent reduction of cytochrome *c* (0.9/min) and is 92% inhibited by SOD. The balance of noninhibitable cytochrome *c* reductase activity (about 10%) was also observed under rigorously anaerobic conditions.

In contrast to these flavoproteins, ALR-mediated aerobic reduction of cytochrome *c* (Figure 10) is only slightly inhibited by a concentration of SOD that was shown in a separate experiment to completely inhibit the reduction of cytochrome in the xanthine/xanthine oxidase superoxide generating system (not shown; see Materials and Methods). Reduction of cytochrome *c* by reduced ALR was followed in a double-mixing stopped-flow spectrophotometer to facilitate the measurement of initial rates (see Materials and Methods). The appreciable background contribution to these rates (shown by the dotted line in Figure 10) is the well-precedented nonenzymatic reduction of cytochrome *c* by thiol compounds (*52*−*54*).

Consistent with this small effect of SOD, anaerobic assays (comparable to those shown in Figure 10) showed less than 10% difference in rates with their aerobic counterparts (not shown). Using the Michaelis−Menten equation to fit the SOD-independent heme reduction rates in the inset gives a $k_{cat}$ of 270 cytochrome *c* molecules reduced/min and a $K_m$ of 10 $\mu$M. To evaluate whether oxygen or cytochrome *c* is a better electron acceptor for ALR, we needed to determine the $K_m$ for oxygen using the DTT concentration (2 mM) employed in Figure 10. Analysis of complete oxygen electrode traces from air saturation to zero oxygen concentration allowed rates to be estimated by drawing tangents to the curve for a range of oxygen concentrations (*23*). The $K_m$ estimated from a Michaelis−Menten plot of the data is about 240 $\mu$M, consistent with a marked slowing of the

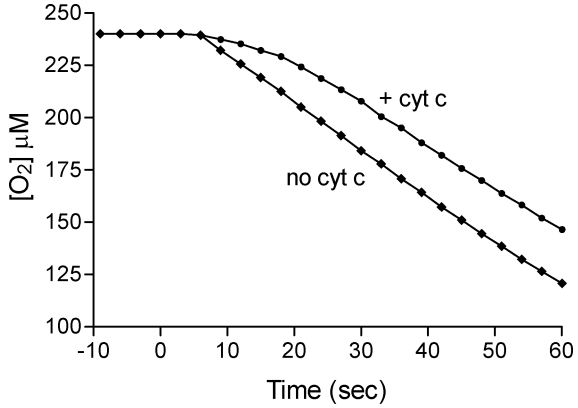


FIGURE 11: Cytochrome *c* inhibits oxygen consumption by ALR. Oxygen consumption was measured in the oxygen electrode after the addition of 2 $\mu$M ALR at time zero to air-saturated buffer containing 2 mM DTT in the presence (circles) or absence (squares) of 100 $\mu$M cytochrome *c*. The oxygen electrode has an intrinsic delay time of 6 s.

oxygen electrode trace as oxygen is depleted. Thus, at least in vitro, oxygen appears to be a poorer substrate than cytochrome *c* by about 100-fold (with $k_{cat}/K_m$ values of 4.2 $\times$ $10^3$ and 4.5 $\times$ $10^5$ $M^{-1}s^{-1}$, respectively). If this is the case, oxidized cytochrome *c* would be expected to suppress the consumption of oxygen by ALR in the presence of DTT. Indeed, Figure 11 shows a significant delay in oxygen consumption (added to the approximate 6 s lag inherent in the sensor electrode). This lag persists until cytochrome *c* is depleted (by direct reduction with ALR and nonenzymatic reduction with DTT as in Figure 10).

*Conclusions*. This paper presents the first detailed examination of the redox behavior of ALR and shows that only 2 reducing equivalents can be easily delivered to the short form of the human protein compared to the 4 electrons expected from the additional presence of the proximal disulfide (C62−65). Similarly, a proteolytic fragment of QSOX containing the ERV/ALR domain was also found to only undergo 2-electron reduction using either dithionite or the deazaflavin light method (*55*). In both examples, the flavin is clearly the center with the most positive redox potential. In neither case are thiolate to flavin charge-transfer complexes observed on 2-electron reduction. Instead, both ALR and the QSOX fragment yield the blue semiquinone during reductive titrations, although only traces are seen in the latter case (*55*).

Identification of the physiological substrates for mammalian ALR is an important ongoing exercise (*17*, *19*, *21*, *38*). In addition to a proposed role in Fe/S traffic (*17*), ALR might contribute in some way to the introduction of disulfides found in proteins residing in the intermembrane space, including thionein (*56*, *57*), TIM10 (*58*), TIM13 (*59*), and superoxide dismutase (*60*). In terms of electron acceptors for ALR, our work suggests that ALR may not necessarily function as a sulfhydryl oxidase in the mitochondrial intermembrane space. Thus, while cytochrome *c* is often used as a nonphysiological oxidant for flavoproteins in vitro, in the present case ALR is located in the same cellular compartment, as almost millimolar concentrations of cytochrome *c* (*61*, *62*). A significant amount of this cytochrome *c* is "free" (*63*) and in its oxidized form (*64*). This abundance of an apparently preferred substrate of ALR contrasts with the 2−10 $\mu$M levels of oxygen that prevail in the mitochondrion of respiring tissues (*65*). Even at air saturation (240 $\mu$M oxygen), 100 $\mu$M oxidized cytochrome *c* strongly suppresses oxygen consumption by ALR (evident from the initial lag in Figure 11).

In sum, these data suggest that cytochrome *c* should be considered as a potential oxidant for ALR in vivo. In this mode ALR-mediated oxidations could then be coupled to the respiratory chain without the generation of hydrogen peroxide observed in the oxidase reaction. Further work will examine the long form of human ALR to see whether the additional N-terminal CxxC motif modulates the redox behavior and catalytic versatility of this interesting and enigmatic flavoenzyme.

## ACKNOWLEDGMENT

We thank Dr. Wolfgang Maret for helpful insights.

## REFERENCES

1. Janolino, V. G., and Swaisgood, H. E. (1975) Isolation and characterization of sulfhydryl oxidase from bovine milk, *J. Biol. Chem. 250*, 2532−2538.
2. Lash, L. H., Jones, D. P., and Orrenius, S. (1984) The renal thiol (glutathione) oxidase. Subcellular localization and properties, *Biochim. Biophys. Acta 779*, 191−200.
3. de la Motte, R. S., and Wagner, F. W. (1987) *Aspergillus niger* sulfhydryl oxidase, *Biochemistry 26*, 7363−7371.
4. Ostrowski, M. C., and Kistler, W. S. (1980) Properties of a flavoprotein sulfhydryl oxidase from rat seminal vesicle secretion, *Biochemistry 19*, 2639−2645.
5. Hoober, K. L., Joneja, B., White, H. B., III, and Thorpe, C. (1996) A sulfhydryl oxidase from chicken egg white, *J. Biol. Chem. 271*, 30510−30516.
6. Thorpe, C., Hoober, K., Raje, S., Glynn, N., Burnside, J., Turi, G., and Coppock, D. (2002) Sulfhydryl oxidases: emerging catalysts of protein disulfide bond formation in eukaryotes, *Arch. Biochem. Biophys. 405*, 1−12.
7. Wittke, I., Wiedemeyer, R., Pillmann, A., Savelyeva, L., Spring, H., and Schwab, M. (2003) Neuroblastoma-derived sulfhydryl oxidase, a new member of the sulfhydryl oxidase/Quiescin6 family, regulates sensitization to interferon gamma-induced cell death in human neuroblastoma cells, *Cancer Res. 63*, 7742−7752.
8. Benayoun, B., Esnard-Fève, A., Castella, S., Courty, Y., and Esnard, F. (2001) Rat seminal vesicle FAD-dependent sulfhydryl oxidase: Biochemical characterization and molecular cloning of a member of the new sulfhydryl oxidase/quiescin Q6 gene family, *J. Biol. Chem. 276*, 13830−13837.
9. Coppock, D. L., Cina-Poppe, D., and Gilleran, S. (1998) The Quiescin Q6 gene (QSCN6) is a fusion of two ancient gene families: thioredoxin and ERV1, *Genomics 54*, 460−468.
10. Hoober, K. L., Glynn, N. M., Burnside, J., Coppock, D. L., and Thorpe, C. (1999) Homology between egg white sulfhydryl oxidase and quiescin Q6 defines a new class of flavin-linked sulfhydryl oxidases, *J. Biol. Chem. 274*, 31759−31762.
11. Lisowsky, T. (1992) Dual function of a new nuclear gene for oxidative phosphorylation and vegetative growth in yeast, *Mol. Gen. Genet. 232*, 58−64.
12. Hagiya, M., Francavilla, A., Polimeno, L., Ihara, I., Sakai, H., Seki, T., Shimonishi, M., Porter, K. A., and Starzl, T. E. (1994) Cloning and sequence analysis of the rat augmenter of liver regeneration (ALR) gene: expression of biologically active recombinant ALR and demonstration of tissue distribution, *Proc. Natl. Acad. Sci. U.S.A. 91*, 8142−8146.
13. Polimeno, L., Lisowsky, T., and Francavilla, A. (1999) From yeast to man−from mitochondria to liver regeneration: a new essential gene family, *Ital. J. Gastroenterol. Hepatol. 31*, 494−500.
14. Hofhaus, G., Lee, J. E., Tews, I., Rosenberg, B., and Lisowsky, T. (2003) The N-terminal cysteine pair of yeast sulfhydryl oxidase Erv1p is essential for in vivo activity and interacts with the primary redox centre, *Eur. J. Biochem. 270*, 1528−1535.
15. Gerber, J., Muhlenhoff, U., Hofhaus, G., Lill, R., and Lisowsky, T. (2001) Yeast ERV2p is the first microsomal FAD-linked sulfhydryl oxidase of the Erv1p/Alrp protein family, *J. Biol. Chem. 276*, 23486−23491.

16. Lee, J., Hofhaus, G., and Lisowsky, T. (2000) Erv1p from *Saccharomyces cerevisiae* is a FAD-linked sulfhydryl oxidase, *FEBS Lett. 477* (1−2), 62−66.
17. Lange, H., Lisowsky, T., Gerber, J., Muhlenhoff, U., Kispal, G., and Lill, R. (2001) An essential function of the mitochondrial sulfhydryl oxidase Erv1p/ALR in the maturation of cytosolic Fe/S proteins, *EMBO Rep. 2*, 715−720.
18. Sevier, C. S., Cuozzo, J. W., Vala, A., Aslund, F., and Kaiser, C. A. (2001) A flavoprotein oxidase defines a new endoplasmic reticulum pathway for biosynthetic disulphide bond formation, *Nat. Cell Biol. 3*, 874−882.
19. Lisowsky, T., Lee, J. E., Polimeno, L., Francavilla, A., and Hofhaus, G. (2001) Mammalian augmenter of liver regeneration protein is a sulfhydryl oxidase, *Dig. Liver Dis. 33*, 173−180.
20. Gross, E., Sevier, C. S., Vala, A., Kaiser, C. A., and Fass, D. (2002) A new FAD-binding fold and intersubunit disulfide shuttle in the thiol oxidase Erv2p, *Nat. Struct. Biol. 9*, 61−67.
21. Wu, C. K., Dailey, T. A., Dailey, H. A., Wang, B. C., and Rose, J. P. (2003) The crystal structure of augmenter of liver regeneration: A mammalian FAD-dependent sulfhydryl oxidase, *Protein Sci. 12*, 1109−1118.
22. Hoober, K. L., Sheasley, S. S., Gilbert, H. F., and Thorpe, C. (1999) Sulfhydryl oxidase from egg white: a facile catalyst for disulfide bond formation in proteins and peptides, *J. Biol. Chem. 274*, 22147−22150.
23. Hoober, K. L., and Thorpe, C. (1999) Egg white sulfhydryl oxidase: Kinetic mechanism of the catalysis of disulfide bond formation, *Biochemistry 38*, 3211−3217.
24. Hoober, K. L., and Thorpe, C. (2002) Flavin-dependent sulfhydryl oxidases in protein disulfide bond formation, *Methods Enzymol. 348*, 30−34.
25. Mairet-Coello, G., Tury, A., Esnard-Feve, A., Fellmann, D., Risold, P. Y., and Griffond, B. (2004) FAD-linked sulfhydryl oxidase QSOX: topographic, cellular, and subcellular immunolocalization in adult rat central nervous system, *J. Comput. Neurol. 473*, 334−363.
26. Amiot, C., Musard, J. F., Hadjiyiassemis, M., Jouvenot, M., Fellmann, D., Risold, P. Y., and Adami, P. (2004) Expression of the secreted FAD-dependent sulfydryl oxidase (QSOX) in the guinea pig central nervous system, *Mol. Brain Res. 125*, 13−21.
27. Coppock, D., Kopman, C., Gudas, J., and Cina-Poppe, D. A. (2000) Regulation of the quiescence-induced genes: quiescin Q6, decorin, and ribosomal protein S29, *Biochem. Biophys. Res. Commun. 269*, 604−610.
28. Sevier, C. S., and Kaiser, C. A. (2002) Formation and transfer of disulphide bonds in living cells, *Nat. Rev. Mol. Cell Biol. 3*, 836−847.
29. Becher, D., Kricke, J., Stein, G., and Lisowsky, T. (1999) A mutant for the yeast scERV1 gene displays a new defect in mitochondrial morphology and distribution, *Yeast 15*, 1171−1181.
30. Klissenbauer, M., Winters, S., Heinlein, U. A., and Lisowsky, T. (2002) Accumulation of the mitochondrial form of the sulphydryl oxidase Erv1p/Alrp during the early stages of spermatogenesis, *J. Exp. Biol. 205*, 1979−1986.
31. Lu, C., Li, Y., Zhao, Y., Xing, G., Tang, F., Wang, Q., Sun, Y., Wei, H., Yang, X., Wu, C., Chen, J., Guan, K. L., Zhang, C., Chen, H., and He, F. (2002) Intracrine hepatopoietin potentiates AP-1 activity through JAB1 independent of MAPK pathway, *FASEB J. 16*, 90−92.
32. Wang, Y., Lu, C., Wei, H., Wang, N., Chen, X., Zhang, L., Zhai, Y., Zhu, Y., Lu, Y., and He, F. (2004) Hepatopoietin interacts directly with COP9 signalosome and regulates AP-1 activity, *FEBS Lett. 572*, 85−91.
33. Wang, G., Yang, X., Zhang, Y., Wang, Q., Chen, H., Wei, H., Xing, G., Xie, L., Hu, Z., Zhang, C., Fang, D., Wu, C., and He, F. (1999) Identification and characterization of receptor for mammalian hepatopoietin that is homologous to yeast ERV1, *J. Biol. Chem. 274*, 11469−11472.
34. Gandhi, C. R., Kuddus, R., Subbotin, V. M., Prelich, J., Murase, N., Rao, A. S., Nalesnik, M. A., Watkins, S. C., DeLeo, A., Trucco, M., and Starzl, T. E. (1999) A fresh look at augmenter of liver regeneration in rats, *Hepatology 29*, 1435−1445.
35. Li, Y., Li, M., Xing, G., Hu, Z., Wang, Q., Dong, C., Wei, H., Fan, G., Chen, J., Yang, X., Zhao, S., Chen, H., Guan, K., Wu, C., Zhang, C., and He, F. (2000) Stimulation of the mitogen-activated protein kinase cascade and tyrosine phosphorylation of the epidermal growth factor receptor by hepatopoietin, *J. Biol. Chem. 275*, 37443−37447.
36. Francavilla, A., Hagiya, M., Porter, K. A., Polimeno, L., Ihara, I., and Starzl, T. E. (1994) Augmenter of liver regeneration: its place in the universe of hepatic growth factors, *Hepatology 20*, 747−757.
37. Polimeno, L., Margiotta, M., Marangi, L., Lisowsky, T., Azzarone, A., Ierardi, E., Frassanito, M. A., Francavilla, R., and Francavilla, A. (2000) Molecular mechanisms of augmenter of liver regeneration as immunoregulator: Its effect on interferon-gamma expression in rat liver, *Dig. Liver Dis. 32*, 217−25.
38. Chen, X., Li, Y., Wei, K., Li, L., Liu, W., Zhu, Y., Qiu, Z., and He, F. (2003) The potentiation role of hepatopoietin on AP-1 is dependent on its sulfhydryl oxidase activity, *J. Biol. Chem. 278*, 49022−49030.
39. DuPlessis, E. R., Pellet, J., Stankovich, M. T., and Thorpe, C. (1998) Oxidase activity of the acyl-CoA dehydrogenases, *Biochemistry 37*, 10469−10477.
40. Wu, C. K., Dailey, T. A., Dailey, H. A., Francavilla, A., Starzl, T. E., Wang, B. C., and Rose, J. P. (2000) Expression, purification, crystallization and preliminary x-ray analysis of the augmenter of liver regeneration, *Protein Pept. Lett. 7*, 25−32.
41. Thornton, J. M. (1981) Disulphide bridges in globular proteins, *J. Mol. Biol. 151*, 261−287.
42. Srinivasan, N., Sowdhamini, R., Ramakrishnan, C., and Balaram, P. (1990) Conformations of disulfide bridges in proteins, *Int. J. Pept. Protein Res. 36*, 147−155.
43. Hofhaus, G., and Lisowsky, T. (2002) Sulfhydryl oxidases as factors for mitochondrial biogenesis, *Methods Enzymol. 348*, 314−324.
44. Massey, V., and Palmer, G. (1966) On the existence of spectrally distinct classes of flavoprotein semiquinones. A new method for the quantitative production of flavoprotein semiquinones, *Biochemistry 5*, 3181−3189.
45. Massey, V. (2000) The chemical and biological versatility of riboflavin, *Biochem. Soc. Trans. 28*, 283−296.
46. Williams, C. H., Jr. (1992) Lipoamide dehydrogenase, glutathione reductase, thioredoxin reductase, and mercuric ion reductase-A family of flavoenzyme transhydrogenases, in *Chemistry and Biochemistry of Flavoenzymes* (Müller, F., Ed.) pp 121−211, CRC Press, Boca Raton, FL.
47. Page, C. C., Moser, C. C., and Dutton, P. L. (2003) Mechanism for electron transfer within and between proteins, *Curr. Opin. Chem. Biol. 7*, 551−556.
48. Page, C. C., Moser, C. C., Chen, X., and Dutton, P. L. (1999) Natural engineering principles of electron tunnelling in biological oxidation−reduction, *Nature 402*, 47−52.
49. Massey, V., Strickland, S., Mayhew, S. G., Howell, L. G., Engel, P. C., Matthews, R. G., Schuman, M., and Sullivan, P. A. (1969) The production of superoxide anion radicals in the reaction of reduced flavins and flavoproteins with molecular oxygen, *Biochem. Biophys. Res. Commun. 36*, 891−897.
50. Butler, J., Koppenol, W. H., and Margoliash, E. (1982) Kinetics and mechanism of the reduction of ferricytochrome *c* by the superoxide anion, *J. Biol. Chem. 257*, 10747−10750.
51. Ballou, D., Palmer, G., and Massey, V. (1969) Direct demonstration of superoxide anion production during the oxidation of reduced flavin and of its catalytic decomposition by erythrocuprein, *Biochem. Biophys. Res. Commun. 36*, 898−904.
52. Engman, L., Tunek, A., Hallberg, M., and Hallberg, A. (1994) Catalytic effects of glutathione peroxidase mimetics on the thiol reduction of cytochrome *c*, *Chem.-Biol. Interact. 93*, 129−137.
53. Dikalov, S., Khramtsov, V., and Zimmer, G. (1996) Determination of rate constants of the reactions of thiols with superoxide radical by electron paramagnetic resonance: critical remarks on spectrophotometric approaches, *Arch. Biochem. Biophys. 326*, 207−218.
54. Massey, V., Williams, C. H., Jr., and Palmer, G. (1971) The presence of S degrees-containing impurities in commercial samples of oxidized glutathione and their catalytic effect on the reduction of cytochrome *c*, *Biochem. Biophys. Res. Commun. 42*, 730−738.
55. Raje, S., and Thorpe, C. (2003) Inter-domain redox communication in flavoenzymes of the quiescin/sulfhydryl oxidase family: role of a thioredoxin domain in disulfide bond formation, *Biochemistry 42*, 4560−4568.
56. Maret, W. (2003) Cellular zinc and redox States converge in the metallothionein/thionein pair, *J. Nutr. 133*, 1460S−1462S.
57. Maret, W., and Vallee, B. L. (1998) Thiolate ligands in metallothionein confer redox activity on zinc clusters, *Proc. Natl. Acad. Sci. U.S.A. 95*, 3478−3482.

58. Lu, H., Allen, S., Wardleworth, L., Savory, P., and Tokatlidis, K. (2004) Functional TIM10 chaperone assembly is redox-regulated in vivo, *J. Biol. Chem. 279*, 18952−18958.

59. Lutz, T., Neupert, W., and Herrmann, J. M. (2003) Import of small Tim proteins into the mitochondrial intermembrane space, *EMBO J. 22*, 4400−4408.

60. Field, L. S., Furukawa, Y., O'Halloran, T. V., and Culotta, V. C. (2003) Factors controlling the uptake of yeast copper/zinc superoxide dismutase into mitochondria, *J. Biol. Chem. 278*, 28052−28059.

61. Han, D., Williams, E., and Cadenas, E. (2001) Mitochondrial respiratory chain-dependent generation of superoxide anion and its release into the intermembrane space, *Biochem. J. 353*, 411−416.

62. Hackenbrock, C. R., Chazotte, B., and Gupte, S. S. (1986) The random collision model and a critical assessment of diffusion and collision in mitochondrial electron transport, *J. Bioenerg. Biomembr. 18*, 331−368.

63. Cortese, J. D., Voglino, A. L., and Hackenbrock, C. R. (1995) Persistence of cytochrome *c* binding to membranes at physiological mitochondrial intermembrane space ionic strength, *Biochim. Biophys. Acta 1228*, 216−228.

64. Morgan, J. E., and Wikstrom, M. (1991) Steady-state redox behavior of cytochrome *c*, cytochrome *a*, and CuA of cytochrome *c* oxidase in intact rat liver mitochondria, *Biochemistry 30*, 948−958.

65. Jones, D. P. (1986) Intracellular diffusion gradients of O2 and ATP, *Am. J. Physiol. 250*, C663−C675.

BI0479555